https://doi.org/10.20965/ijat.2022.p0642

Paper:

Enhancing the Shape Complexity in Direct Energy Deposition with Phased Deformation

Srinath Gudur, Suryakumar Simhambhatla†, and N. Venkata Reddy

Department of Mechanical and Aerospace Engineering, Indian Institute of Technology Hyderabad (IITH)
Kandi, Sangareddy, Telangana 502285, India
†Corresponding author, E-mail: ssurya@iith.ac.in
[Received January 9, 2022; accepted March 9, 2022]

Wire-based direct energy deposition (W-DED) techniques in metal additive manufacturing allow part-fabrication at higher deposition rates and lower costs. Given the lack of any support mechanism, these processes face challenges in fabricating overhanging features. The inherent overhang capability of weld-beads and higher-order kinematics can help realize certain complex geometries. However, significant challenges like non-uniform slicing, constrained deposition-torch accessibility, etc., limit the efficacy of these approaches. The present work describes a deformation-aided deposition process designed to overcome some of these limitations and to manufacture complex metallic components. It is based on a sequential combination of deposition and bending processes: a shape fabricated through W-DED deposition is bent to form the required shape. The cycle of deposition and bending is repeated until the final desired geometry is realized. The anisotropic and deterministic behaviors of the deposited components are analyzed in terms of springback and the punch force. Finally, the benefit of current hybrid process is demonstrated through a few illustrative geometries.

Keywords: metal additive manufacturing, wire-based direct energy deposition (W-DED), hybrid additive manufacturing processes, deformation aided deposition process

1. Introduction

Wire-based direct energy deposition (W-DED), also known as wire arc additive manufacturing (WAAM), allows the speedy fabrication of large parts with a high material efficiency. Among the different metal additive manufacturing (AM) processes available, W-DED has the advantages of high deposition rate (approximately 50–100 g/min) [1], lower equipment and material costs, and the possibility to deposit large-scale components with medium complexity.

One major challenge of W-DED is its limited ability to manufacture complex shapes [2]. The sizeable liquid melt pool produced during the deposition of a layer limits the ability to deposit overhangs or to produce complex internal geometries. To some degree, the inherent overhang capability of weld beads can be used to deposit components with small overhangs using parallel slicing and simple 3-axis planar deposition. Larger overhangs can be achieved using higher-order kinematics, either by rotating the substrate or component onto which deposition occurs [3] or by tilting the deposition torch [4]. Kazanas et al. used the technique of tilting the weld-deposition torch to achieve even greater angles via positional welding [5]. Using 5-axis kinematics for weld deposition, Panchagnula and Simhambhatla produced complex metallic structures without using supports [3]. However, such higher-axis kinematics face challenges such as non-uniform slicing, constrained deposition-torch accessibility, and a non-parallel axis of curvature. To overcome these challenges, there is growing interest in developing hybrid approaches that combine additive manufacturing with traditional manufacturing processes, such as forming [6, 7].

Colegrove et al. [8] combined the rolling of deposited beads with WAAM to improve the surface finish and microstructure. Their deposition process was followed by rolling, which included the rolling of the deposited layers using high-pressure rollers. Zhang et al. [9] focused on hybrid deposition and micro-rolling, in which the rolling step followed deposition using rollers mounted immediately behind the torch. The following studies examined the effects of combining rolling with WAAM for different materials: Ti-6Al-4V by Martina et al. [10], 45 steel by Hai-ou et al. [11], 2319 and 5087 aluminum alloys by Gu et al. [12], and Inconel 718 by Xu et al. [13]. Lateral rolling, performed in addition to top rolling, in the form of a metamorphic rolling mechanism (MRM), was introduced by Xie et al. to improve the surface quality [14]. Furthermore, in the compound arc and vibration shock forging rolling (CAVSFR) introduced by Ma et al. [15], a roller loaded with a static force and shock vibrations is placed behind the deposition torch. Both the roller and the torch are then moved synchronously. The vibrations are transmitted to the molten pool, thereby inducing micro-self-forging in the molten pool. As the molten pool solidifies, the advancing roller rolls over the solidified surface and forges the top surface.

In all the approaches described above, deformation occurs only on the deposited bead. The focus is mainly

on enhancing the material properties through grain refinement and on improving the surface quality of the deposited WAAM components. One notable exception is Li and Rapthadu [16], who used a bending operation to produce non-flat substrates. Their deposition was performed at different locations, depending on the requirements to deposit overhangs. However, that work was concerned with bending the substrate rather than the deposited part.

The present work describes a bending-aided deposition process for manufacturing complex metallic components. This process involves bending a deposited component into the required shape. Subsequent depositions can be applied onto the bent component, which can be bent again. This process of deposition and bending is repeated until the final desired geometry is obtained.

The process is demonstrated using a deposition station retrofitted onto a 3-axis computer numerical control (CNC) machine for deposition, and a bending station consisting of a purpose-built hydraulic press used to bend the deposited components. At the deposition stage, as the build progresses, the components undergo a complex thermal evolution [17]. This may lead to microstructural heterogeneity in the deposited metal components [18]. Hence, we first analyzed the deformation of the deposited components to understand their anisotropic characteristics. This also involved using numerical simulations and experiments to predict springback and the punch force for machined deposited components. We then present several illustrative examples for demonstration and validation. The process was implemented here with an arc-welding-based W-DED setup, but it is also applicable to laser-based W-DED [19].

2. Methodology and Setup of the Deformation-Aided Deposition Process

This section details the methodology of the deformation-aided deposition process and the setup used for its implementation. In its conceptual form, the process consists of two main stations. The first station, designed for deposition, involves a gas metal arc welding (GMAW) torch. The second station performs bending with a hydraulic press, employing customized dies and punches. The component deposited in the first station can be transferred to the second station for bending into the required shape or geometry. It can then be returned to the deposition station for further processing. The desired shape can be obtained by reiterating this protocol. The concept is outlined by the three stages depicted in **Fig. 1**. After deposition (**Fig. 1(a)**) the component is mounted onto the bending setup (**Fig. 1(b)**). The resultant component is shown in **Fig. 1(c)**.

Deposition was performed using a GMAW welding torch (Fronius, Model: CMT 4000 Advanced) mounted on a 3-axis machining center, as shown in **Fig. 2**. **Fig. 3** shows the purpose-built hydraulic press used to bend the deposited component. The maximum load capacity of the hydraulic press was 20 kN. Several dies and punches

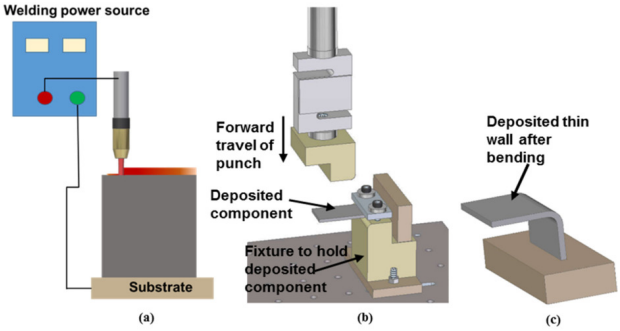

Fig. 1. Deformation-aided deposition process (a) deposition using CMT, (b) bending using hydraulic press, (c) deformation aided deposition component.

can be attached to the press, as required. The transfer of the component between the stations can, in principle, be automated. However, in the current experimental setup, this transfer was executed manually, our focus being to demonstrate the feasibility of complex geometry fabrication by combining deposition and bending. This feasibility with respect to the edge-bending behavior and its conformity with finite-element analysis is presented in the next section.

3. Deformation Analysis of Deposited Components

Geometries fabricated by deposition usually display properties different from those manufactured with more traditional techniques. During deposition, as the build progresses, the components acquire a complex repetitive thermal history that includes directional heat extraction and variable cooling rates [17], with repeated remelting and re-solidification of layers. This produces microstructural heterogeneity in the deposited metal components [18]. This section presents a deformation analysis of the deposited components designed to study their anisotropic characteristics.

The deformation analysis was carried out in two stages, consisting of (a) the tensile testing of the deposited parts to understand the role of orientation and location; and (b) edge bending tests and their comparison with numerical predictions to demonstrate deterministic nature of the deposition process.

The analysis was performed on a thin-wall geometry with dimensions 135 mm $\times$ 135 mm $\times$ 5.5 mm. ER70S6 wire (C: 0.075%; Mn: 1.22%; Si: 0.67%; P: 0.01%; S: 0.014%; Fe: 98.011%) with a 0.8 mm diameter was used as the feedstock for deposition. An EN8 block (C: 0.4%; Mn: 0.63%; Si: 0.22%; P $\leq$ 0.05%; S $\leq$ 0.05%; Fe: 98.65%) with dimensions 200 mm $\times$ 75 mm $\times$ 12 mm was used as the substrate. **Fig. 2** shows the experimental setup used for deposition. The process parameters used for the deposition are listed in **Table 1**. The deposition direction was re-

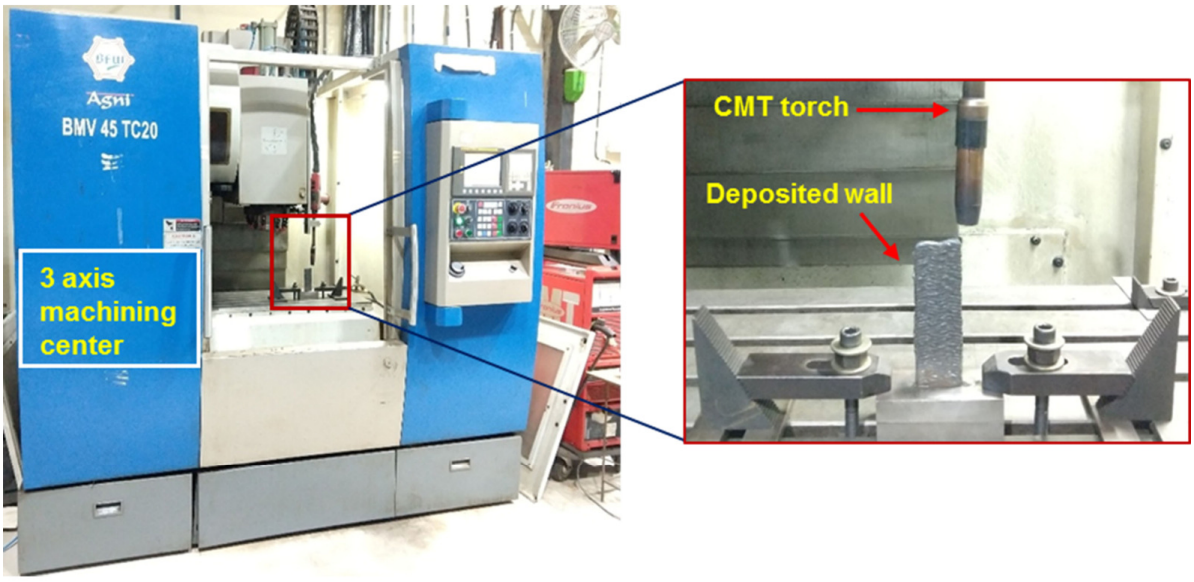

Fig. 2. Experimental setup for deposition.

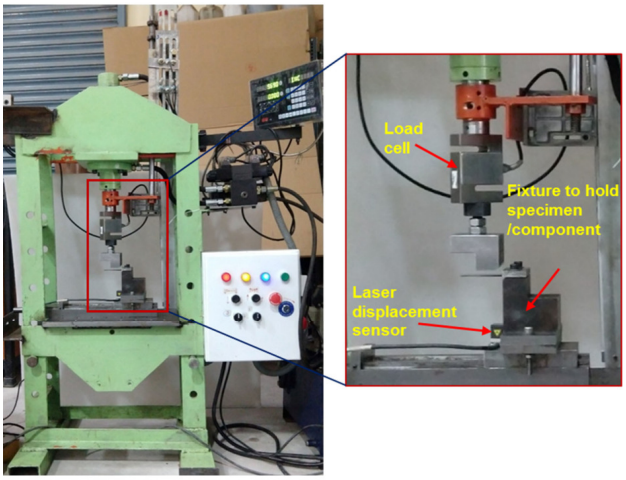

Fig. 3. Purpose-built hydraulic press for deformation.

Table 1. Deposition parameters.

Current	120 A
Voltage	15.3 V
Wire feed speed	10.6 m/min
Travel speed	0.6 m/min
Wire diameter	0.8 mm
Shielding gas	82 % Ar + 18 % CO_2
Gas flow rate	10 litres/min
Substrate dimensions	200 mm × 75 mm × 12 mm
Number of layers	78
Layer thickness (average)	1.73 mm
Length of each pass	135

versed for every alternating layer (zigzag strategy) to minimize start/stop effects. To maintain consistency, each new layer was deposited when the previous layer reached 93°C. (This follows earlier studies by Panchagnula et al., which proved that 93°C was the optimal preheating temperature [20].) A deposited wall height of 135 mm was realized in 78 layers. The average measured wall width was approximately 5.5 mm. The specimens required for the deformation analysis were extracted from this thin-wall geometry, the details of which are presented in the following sections.

3.1. Tensile Properties

The orientation and location of a deposited component are two aspects of interest when judging its properties. The orientation arises from the layered nature of the build, and the location is due to the varying thermal conditions across the layers. Hence, tensile specimens were extracted from the thin walls mentioned above to evaluate the influence of these aspects. We used a scaled version of the ASTM A370 standard tensile test specimen with a gauge length of 18 mm.

In typical components built by deposition, as the build progresses, the cooling rate of the layers varies with their distance from the substrate. This may affect the material properties across the built parts. According to earlier studies by Kulkarni et al. [17], built parts can be categorized into three main regions: (a) bottom layers close to the substrate, which undergo rapid solidification owing to predominant conduction; (b) middle layers with a consistent grain structure resulting from resolidification; and (c) top layers that undergo rapid solidification because of predominant convection losses. Accordingly, specimens were extracted from the bottom, middle, and top layers.

The middle-region specimens were further segregated based on their orientation and layout relative to the deposited layer. Specimens with three orientations were extracted: (a) along the deposition direction, (b) along the build direction, and (c) at an angle of 45° relative to the deposition direction. Furthermore, to understand the in-

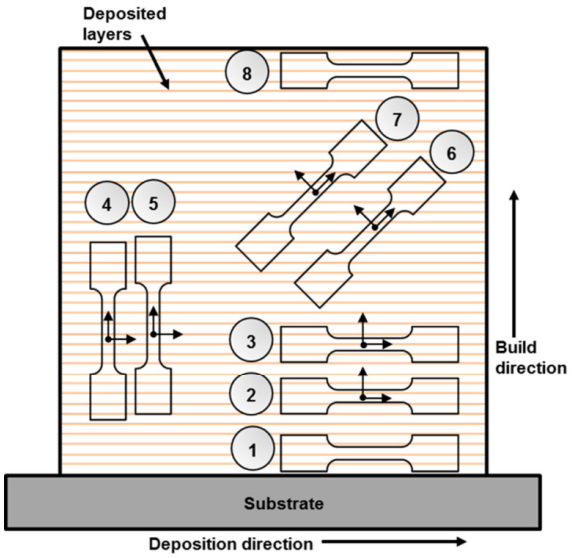

Fig. 4. Scheme of sample collection for tensile test.

fluence of varying thermal conditions across a layer during its solidification, two additional specimens were extracted: one with its center in the middle of the layer, and the other with its center at the edge, as shown in **Fig. 4**. The specimen inventory can thus be summarized as follows:

- Bottom region (specimen #1)
- Middle region
  - Along the deposition direction
    - Specimen center in the middle of the layer (specimen #2)
    - Specimen center at the edge of the layer (specimen #3)
  - Along the build direction
    - Specimen center in the middle of the layer (specimen #4)
    - Specimen center at the edge of the layer (specimen #5)
  - 45° relative to the deposition direction
    - Specimen center in the middle of the layer (specimen #6)
    - Specimen center at the edge of the layer (specimen #7)
- Top region (specimen #8)

Figure 4 illustrates the scheme used for collecting the tensile specimens. The above pattern was repeated three times, to obtain average values and errors. Tensile tests were carried out on a universal testing machine (Biss, Model: Nano) with a strain rate of 0.001 s^{-1}.

The stress-strain data obtained from the tensile tests are presented in **Fig. 5**. The variations in the yield strength and percentage elongation of all the specimens are shown

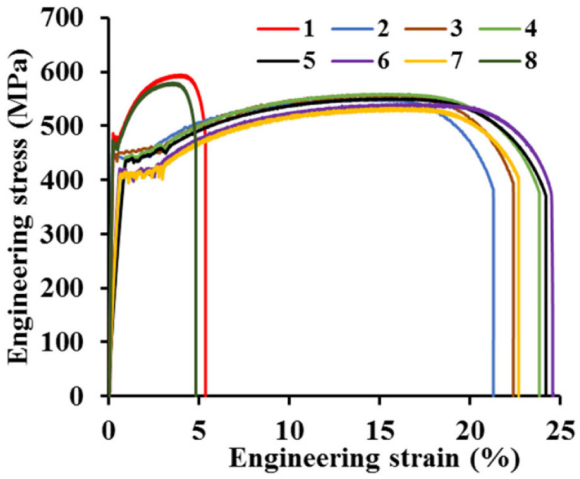

Fig. 5. Engineering stress-strain curves for specimens #1–#8.

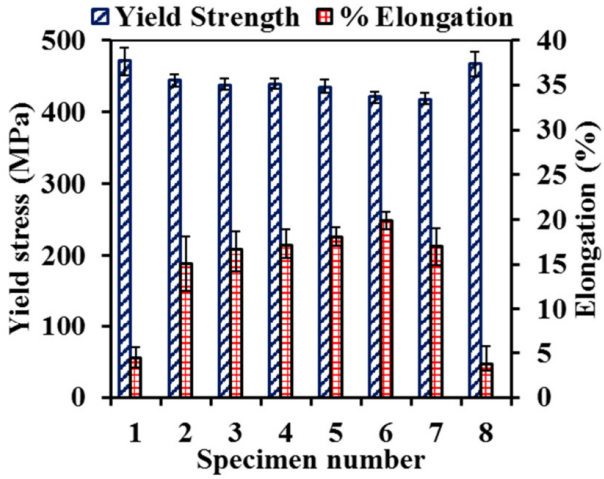

Fig. 6. Yield strength and percentage elongation for specimens #1–#8.

in **Fig. 6**. Specimens #1 and #8 (i.e., those taken from the bottom and top regions, respectively) stand out distinctly from the rest. This is likely due to the rapid solidification in these regions. The yield strengths of specimens #2–#7 ranged from 418 to 444 MPa, and the average of the individual deviations of the case was 16.45 MPa. Hence, the difference between specimens #2 and #7 is of the order of the experimental variation. In other words, this suggests that the middle-region specimens display a similar flow behavior. The percentage elongation displayed an analogous behavior (range: 15.11%–19.88%; average of individual deviations: 3.63%). Thus, these tensile tests revealed that the bending loads required to bend a deposited component are independent of the bending location and direction, except for the bottom and top regions. These two regions exhibited a lower percentage of elongation, indicating a lower bendability. Hence, specimens from the middle region were used in all the subsequent studies.

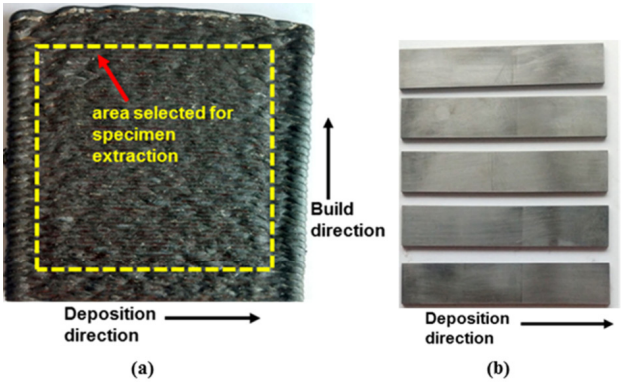

Fig. 7. Scheme for bending specimen extraction: (a) deposited geometry (after separating from substrate), (b) bending specimen (dimensions 100 mm × 20 mm × 2 mm).

3.2. Edge-Bending Behavior

The next step in the deformation analysis involved the edge bending of the specimens. The objective was to demonstrate that the behavior of AM components can be modelled and predicted deterministically. Hence, experimental results were compared with corresponding numerical simulations. Details of the experiments and numerical simulations are described in the following subsections.

3.2.1. Experimental Procedure

Flat specimens of length 100 mm and width 20 mm were chosen for experiments. To maintain consistency across samples, they were machined to a thickness of 2 mm. The samples were extracted from the middle portion of the deposited wall, i.e., avoiding the bottom and top regions (∼15 mm from the bottom and ∼15 mm from the top) for reasons discussed above. **Fig. 7** shows the as-built geometry and the extracted specimens.

The edge bending of the samples was executed using the customized setup shown in **Fig. 3**. It is important to measure the bending loads, punch-stroke values, and springback during these analyses. Hence, a custom setup was developed to mount the necessary sensors. The punch was powered by a hydraulic press and equipped with a load cell (Adi Artech, Model: 20210, with a capacity of ∼20 kN) for the force measurements. A National Instruments (NI) data acquisition (DAQ) system with an NI-9210 input module was used to record the output from the load cell. The punch and die arc radii were both 6 mm. The clearance between the die and punch could be varied by controlling the die location. The motion of the punch was monitored using an inductive proximity sensor. A laser displacement sensor (Micro-Epsilon, Model: ILD1320-100) was used to monitor the specimen displacements during bending. These displacements were used to calculate the final bend angles and the springback.

After mounting the specimen onto the lower die using a clamping plate, the punch was moved downwards to bend it. It was then retracted immediately after the target stroke value was reached. A blank holding force of 16 kN was maintained throughout the experiments.

3.2.2. Numerical Simulations

Three-dimensional finite-element (FE) analyses were conducted to predict the bending force and springback during edge bending. This was carried out in Abaqus/Standard by using an implicit method. The material properties used for the FE simulations were based on the tensile test data presented in Section 3.1. A specimen with dimensions 100 mm × 20 mm × 2 mm was modelled as an elastoplastic material, and its stress-strain relationship was expressed as $\sigma = 864\varepsilon^{0.14}$ MPa. The punch and die were modelled as analytical rigid bodies. The contacts between the punch, die, and sheet were modelled as surface-to-surface contacts with a friction coefficient of 0.2 [21]. A schematic edge-bending assembly is outlined in **Fig. 8**. The specimen was discretized using C3D8R brick elements. A fine discretization (0.25 mm × 0.25 mm) was used near the die arc region after performing a mesh convergence study, and a coarse discretization (2 mm × 0.25 mm) was used in the remaining region. The specimen thickness was discretized into six elements.

The sheet material was assumed to yield according to the von Mises criterion with elastoplastic isotropic hardening. All degrees of freedom of the die were arrested. The punch was allowed to move in the Y-direction to apply the displacement, while the remaining degrees of freedom of the punch were arrested. The sheet was held on the die using a clamping plate, onto which the blank holding force was applied.

3.2.3. Comparison of Experimental and Numerical Results

Experiments were performed at two different punch and die clearance values (C = 4 and 12 mm) for different punch stroke values (4, 8, 12, and 16 mm). These exact scenarios were simulated numerically. **Fig. 9** shows the edge bending of one specimen, and **Fig. 10** shows several bent specimens after unclamping. All experiments were repeated three times to obtain average values. **Table 2** lists the FE simulation and experimental results.

Figure 11 compares the springback corresponding to clearance values of 4 and 12 mm. Springback refers to the phenomenon whereby the metal tends to recover its original configuration when the bending force is removed. As shown in **Fig. 11**, springback increases with increasing punch stroke for a given punch and die clearance. Furthermore, a lower clearance results in less springback for a given punch stroke value.

Figure 12 compares the punch force obtained by FE simulation and experiment, for the case of a punch and die clearance C = 12 mm and punch stroke = 12 mm, showing good agreement. **Fig. 11** indicates a similar concurrence for all the other cases as well. The accurate prediction of springback helps to achieve the required bend angles.

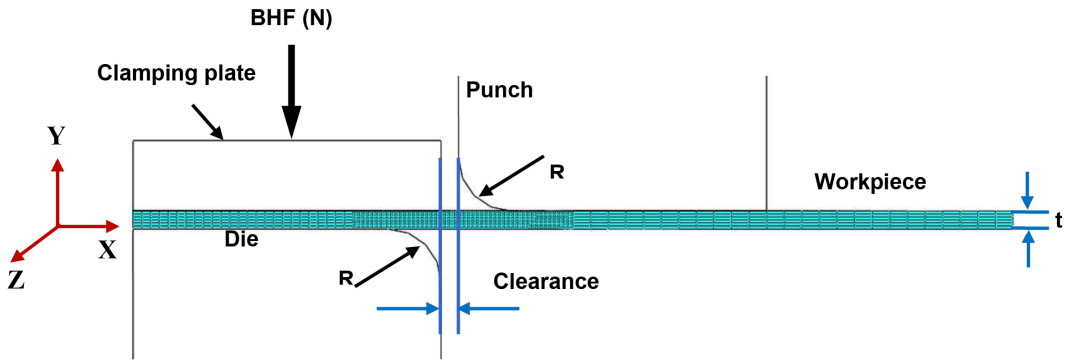

Fig. 8. FE simulation model (thickness $t = 2$ mm; die and punch radius R = 6 mm; clearance C = 2, 4, or 12 mm).

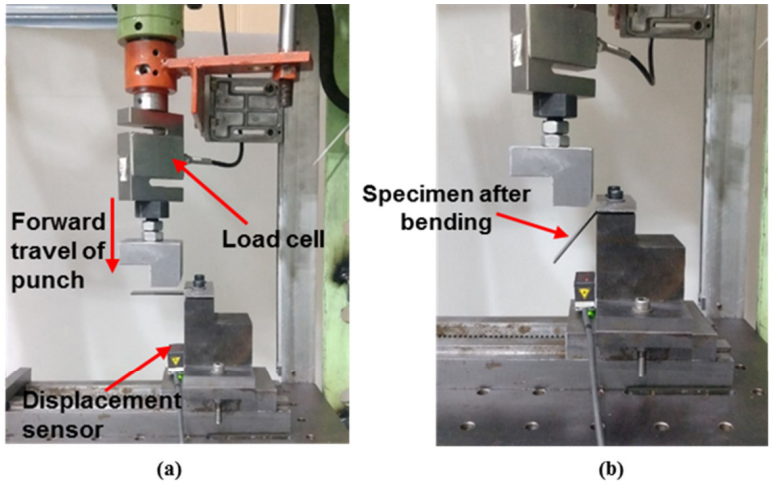

Fig. 9. Edge bending of a W-DED specimen (a) before punch movement, (b) punch retracted after punch stroke.

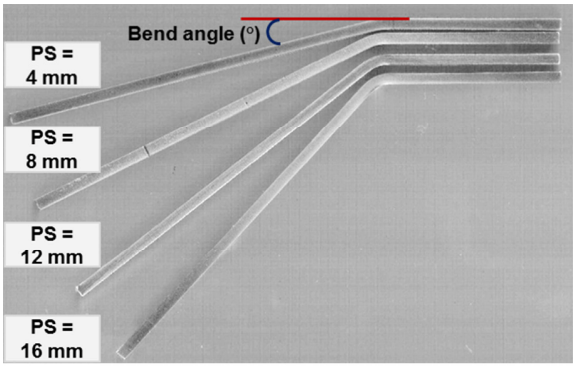

Fig. 10. Bent samples for different punch strokes.

Table 2. Comparison of FE simulation and experimental results.

S. No	Clearance, C (mm)	Punch stroke, PS (mm)	Final bend angle (°)		Springback (°)		Max. Punch force (N)	
			FEM	Expt.	FEM	Expt.	FEM	Expt.
1	4	4	15.5	15.0	1.9	1.6	981	1070
2	4	8	32.7	29.7	2.0	1.9	1078	1121
3	4	12	44.3	40.1	2.2	2.0	1186	1134
4	4	16	54.6	49.3	2.5	2.8	1189	1154
5	12	4	8.8	9.7	2.7	2.9	535	537
6	12	8	19.7	18.3	2.9	3.2	577	556
7	12	12	29.8	27.7	3.0	3.3	578	583
8	12	16	38.7	36.5	3.3	3.7	579	586
9	2	L-bend	87.0	86.5	3.0	3.5	1750	1623

The deterministic nature of the deposited samples was further validated by considering the case of L-shaped bending. Similar to earlier samples, this sample was machined to a thickness of 2 mm after deposition. To achieve an L-bend, the clearance between the punch and the die must be maintained at the specimen thickness, i.e., 2 mm. The punch stroke was not restricted, but was allowed to cover the entire span. The trend of the simulated punch force agrees well with the experimentally measured punch force, as shown in **Fig. 13**. The experimental and numerical results for the springback factor vary by 0.6%.

Edge bending was also performed at different angles on the components built by deposition. A straight wall of length 100 mm and width 40 mm was deposited using the deposition setup shown in **Fig. 2**. The deposi-

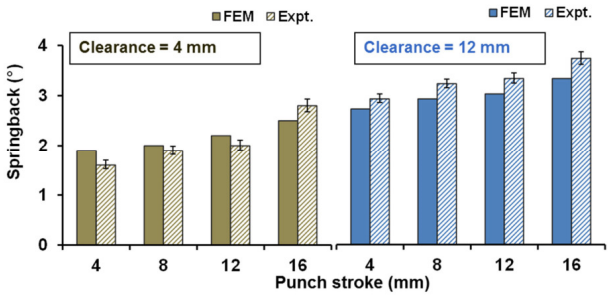

Fig. 11. Springback comparison.

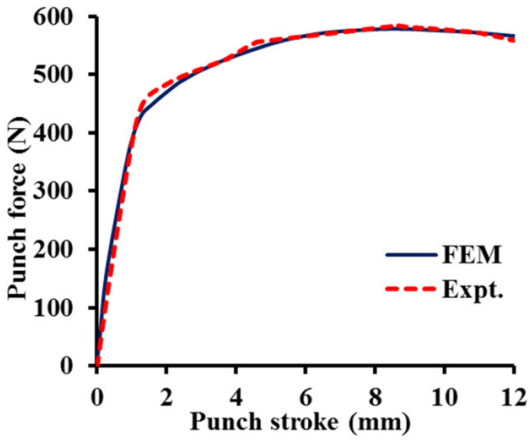

Fig. 12. Punch force comparison for clearance, C = 12 mm, and punch stroke = 12 mm.

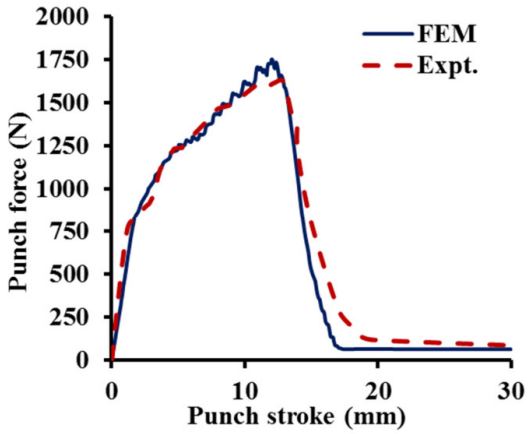

Fig. 13. Punch force comparison for validation case of L-bend.

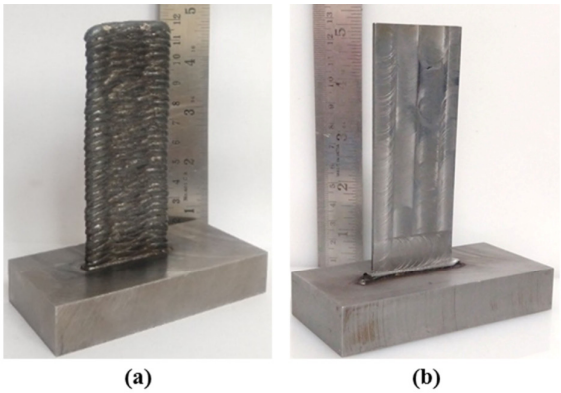

Fig. 14. Thin wall deposited geometry of 100 mm length and 40 mm width (a) as deposited, (b) after machining.

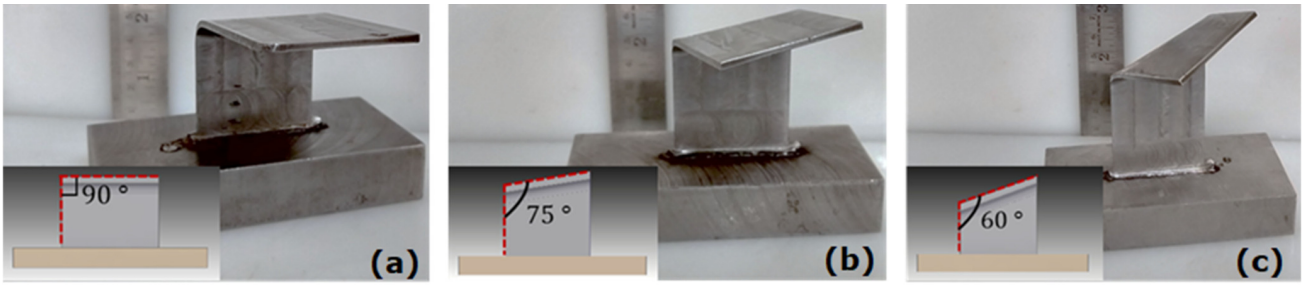

Fig. 15. Machined W-DED thin walls after bending (a) angle = 90°, (b) angle = 75°, (c) angle = 60°.

tion process parameters were the same as those listed in **Table 1**. The deposited wall was machined without being separated from the substrate. The deposited and machined thin-walled geometries are shown in **Fig. 14**. The machined samples were subjected to bending to produce various bend angles θ, as depicted in **Fig. 15**. The geometries shown in **Figs. 15(a)–(c)** were clamped onto the bending setup, giving $\theta = 90°$, 75°, and 60°, respectively. These scenarios were numerically simulated to compare with the experimentally measured punch forces and the springback.

Table 3 shows good agreement between the FE simulation and experimental results, which confirms the predictability of the deposited samples for bending.

4. Case Study: Fabrication of Complex Illustrative Geometries

The deformation analysis of the components manufactured using deposition was established in the previous sections. The following sections provide several il-

Table 3. Comparison of FE simulation and experimental results for machined W-DED components.

Geometry	Springback (°)		Punch force (N)	
	FEM	Expt.	FEM	Expt.
15a	3.5	4.4	4292	3906
15b	0.9	1.3	4271	3886
15c	1.7	1.5	4905	4404

lustrative case studies to demonstrate the benefits of the deformation-aided deposition process for achieving complex geometries. These geometries, labelled A–E in **Fig. 16**, were chosen to illustrate the different challenges faced while fabricating components using established deposition approaches. These challenges can be classified as follows.

- Overhanging features: As a consequence of the layer-by-layer approach of deposited components, new deposition can only occur on top of a previous layer. Although some small gradual angles can be realized using the inherent overhang capability of the process, this approach is inapplicable to large and abrupt overhangs. Geometries A–E represent this challenge.
- Non-parallel axis of curvature of overhang: If the axes of curvature of the overhangs are mutually parallel, these overhangs can be realized by suitably tilting and aligning the base plate using a fourth axis addition to the 3-deposition axes. However, if these axes are not parallel, an additional rotary axis is required to realize the components. Whereas geometry C can be managed with 4-axis kinematics, geometries D and E need 5-axis movement.
- Nonuniform slicing: Uniform slicing is able to produce a desired shape over which the material progression is consistent, albeit with higher-order kinematics. However, in cases where the curvature is not parallel to the deposition layers, slicing based on geometrical features is required. In some cases, even adaptive control with variable wire-feed rates and travel speeds may be required. This particular challenge is illustrated with geometry B.
- Constrained torch accessibility: The accessibility of the torch for subsequent deposition is a challenge for geometries with sharp and narrow features, in particular hollow, enclosed cavities, as illustrated in geometries A and E.

Certain instances of the challenges described above can be addressed using higher-order kinematics, slicing, and path planning. However, the combination of these challenges may be problematic. On the other hand, the deformation-aided deposition process may address these challenges through its greater flexibility. These challenges and their tractability by different approaches are summarized in **Table 4**. While this process significantly widens the scope of possible geometries, shape deformations must lie within limits imposed by the material to be achievable, and they must allow access by the punch and fixture setup.

Deformation-aided deposition couples two separate processes, namely deposition and bending. A deposited component undergoes bending into the required shape through the application of a load at specific target locations. This process of deposition and bending is reiterated until the final desired geometry is obtained. The finished components obtained by this protocol are shown in **Fig. 17**. The methodology and fabrication process are described below.

Figure 18 describes the various stages in manufacturing component A by deformation-aided deposition. In **Fig. 18(a)**, a hollow square box was deposited using W-DED and the parameters listed in **Table 2**. A straight wall of the required length was then deposited on top of one of the walls, as shown in **Fig. 18(b)**. It was subsequently bent with the help of the hydraulic press (**Fig. 18(c)**), giving the finished shape shown in **Fig. 18(d)**.

Figure 19 depicts the manufacturing of component B, which features an inclination in two different planes. A thin wall is first deposited using W-DED (**Fig. 19(a)**). It is then mounted onto the bending setup at the required angle (**Fig. 19(b)**). A bending load is then applied using a punch with a hydraulic press (**Fig. 19(c)**), giving the finished component (**Fig. 19(d)**).

Figure 20 illustrates the manufacturing of component D, which features two mutually perpendicular bending axes. A thin wall, first deposited using W-DED (**Fig. 20(a)**), is bent by applying loads at the target location using the hydraulic press, as shown in **Fig. 20(b)**. Subsequent deposition onto the bent component was carried out to obtain the geometry shown in **Fig. 20(c)**. This wall was again bent (**Fig. 20(d)**) to produce the finished geometry presented in **Fig. 20(e)**.

A similar methodology was adopted for components C (**Fig. 21**) and E (**Fig. 22**). Taken together, these examples demonstrate the versatility of the deformation-aided deposition process. As the setup, in its present form, does not allow for displacement measurements of non-planar shapes, as in **Figs. 16(a)** and **(e)**, the scope of the case studies was limited to assessing the qualitative viability of the geometries.

5. Conclusions

This study presented a novel hybrid deformation-aided deposition process for manufacturing complex metallic components. After describing the design and development of the setup used to demonstrate the process, we analyzed the anisotropic and deterministic behavior of the deposited components in terms of springback and the punch force.

The deformation of the deposited components was first

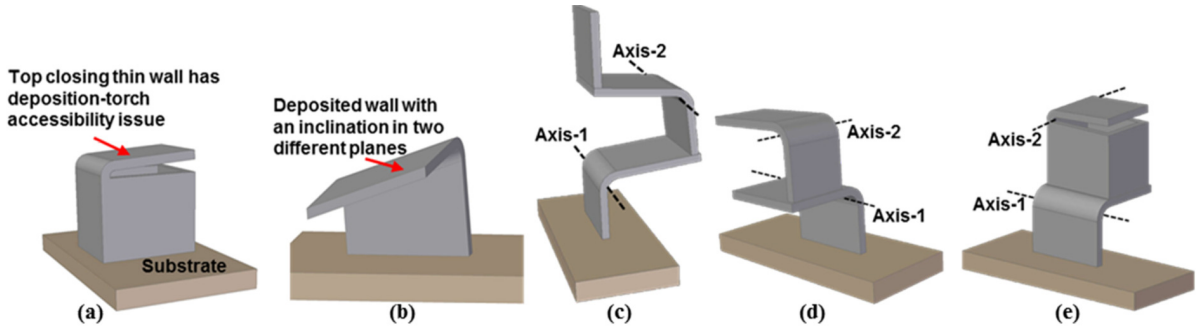

Fig. 16. Geometries illustrating different fabrication challenges (a)–(e) indicating geometries A–E.

Table 4. Fabrication feasibility for components with different types of constraints.

S. No.	Geometries	Constraints / Geometrical Challenge				Feasibility by only Deposition			Feasibility by Deposition + Bending
		Overhanging features	Non-parallel axis of curvature of overhang	Non-uniform slicing	Constrained torch accessibility	3-Axis	4-Axis	5-Axis	
1	Geometry-A	✓	✗	✗	✓	✗	✗	✗	✓
2	Geometry-B	✓	✗	✓	✗	✗	✗	✗	✓
3	Geometry-C	✓	✗	✗	✗	✗	✓	✓	✓
4	Geometry-D	✓	✓	✗	✗	✗	✗	✓	✓
5	Geometry-E	✓	✓	✗	✓	✗	✗	✗	✓

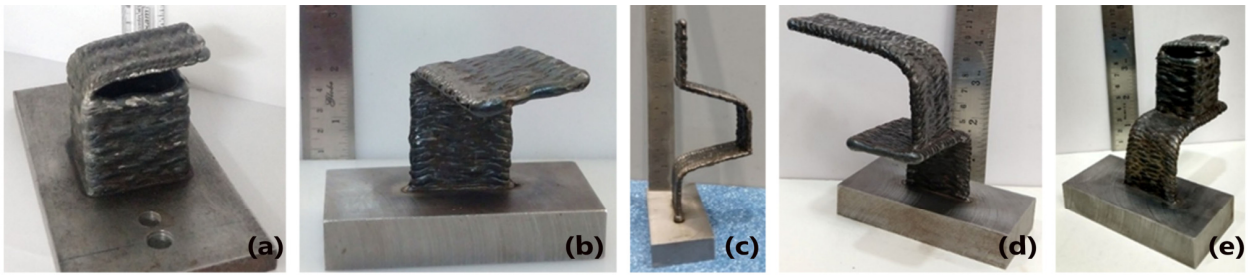

Fig. 17. Complex geometries fabricated using the deformation-aided deposition process: (a)–(e) indicating components A–E, respectively.

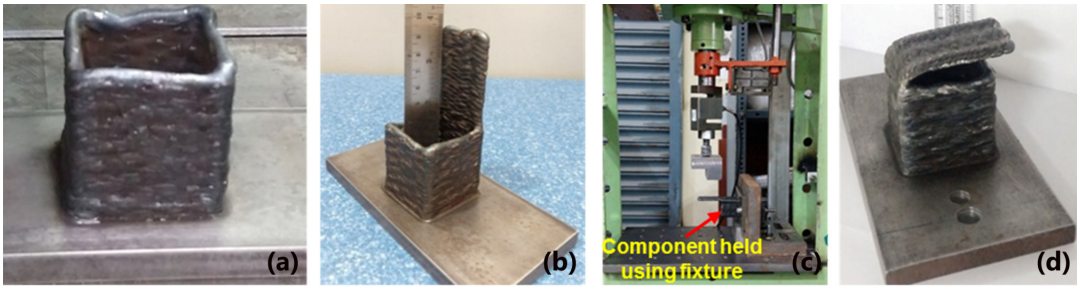

Fig. 18. Stages in manufacturing component A using the deformation-aided deposition process: (a) first deposition of a square box of dimensions 40 mm × 40 mm × 40 mm, (b) second deposition of thin wall on top of one of the walls of the square box, (c) bending of the thin wall to obtain a hollow square box, (d) finished component.

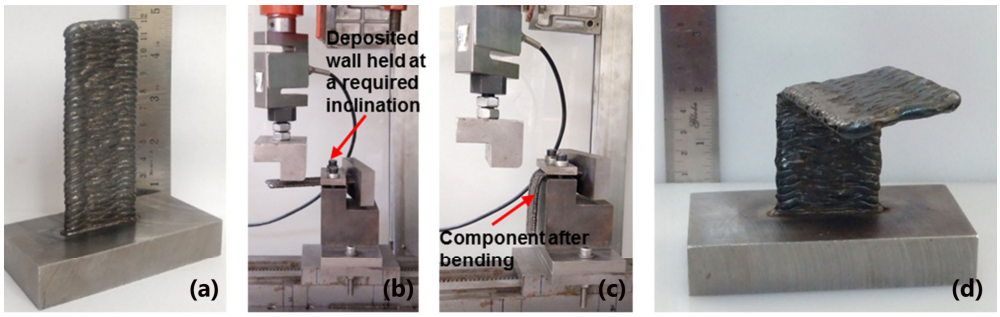

Fig. 19. Stages in manufacturing component B using the deformation-aided deposition process: (a) first thin-wall deposition of width = 40 mm and height = 100 mm, (b) deposited thin wall held at a required inclination, (c) bending using hydraulic press, (d) finished component.

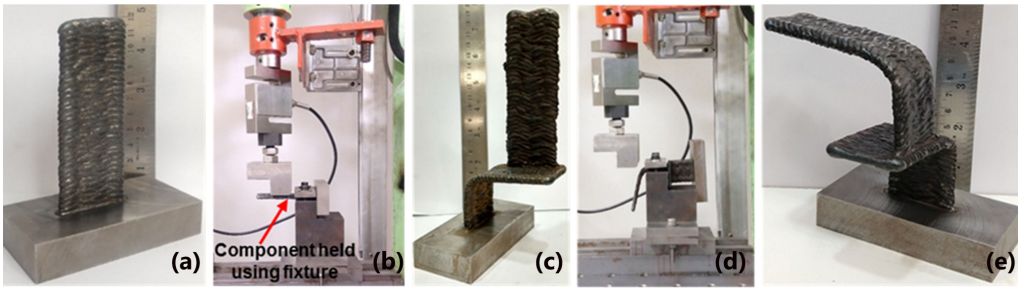

Fig. 20. Stages in manufacturing component D using the deformation-aided deposition process: (a) first thin-wall deposition of width = 40 mm and height = 100 mm, (b) first bending using the hydraulic press, (c) second deposition, (d) second bending, (e) finished component.

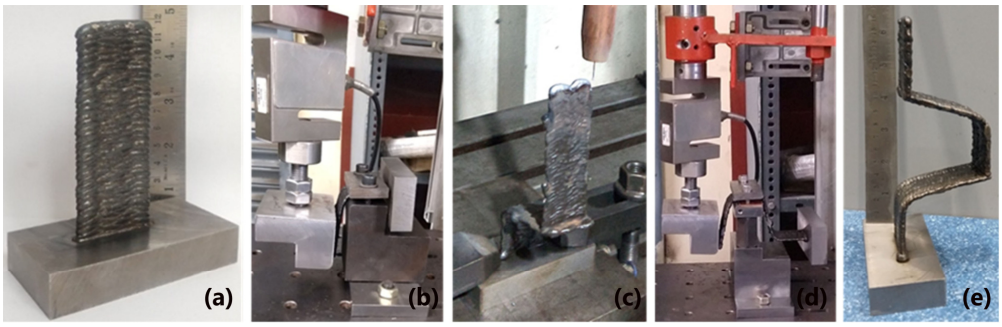

Fig. 21. Stages in manufacturing component C using the deformation-aided deposition process: (a) first thin-wall deposition of width = 40 mm and height = 100 mm, (b) first bending using the hydraulic press, (c) second thin-wall deposition, (d) second bending, (e) finished component.

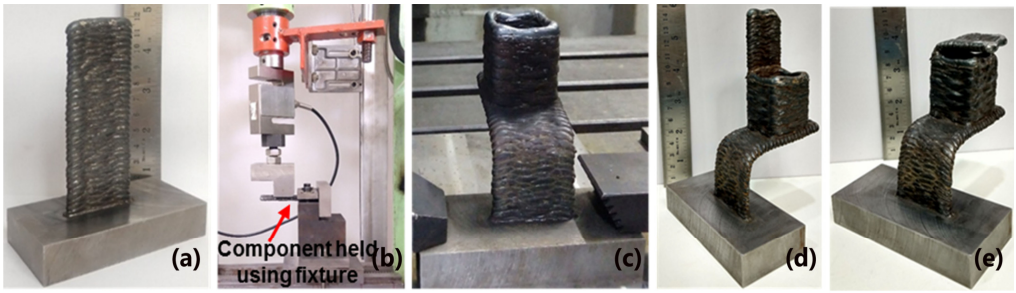

Fig. 22. Stages in manufacturing component E using the deformation-aided deposition process: (a) first thin-wall deposition of width = 40 mm and height = 100 mm, (b) first bending using the hydraulic press, (c) second deposition of a square box, (d) third deposition of a thin wall, (e) finished component after bending the top thin wall.

analyzed to provide an understanding of their anisotropic characteristics. Excluding the extreme top or bottom regions of the deposition, tensile tests indicated that the mechanical behavior is relatively independent of the bending location and direction. Subsequently, edge-bending tests were conducted and their outcomes were compared with numerical predictions. Their good agreement confirms the deterministic nature of the deposition process.

Finally, we demonstrated the appeal and benefits of this hybrid process through a few illustrative geometries, thereby establishing the efficacy of combining bending and deposition processes to produce complex shapes.

Acknowledgments

This work was supported by Advanced Manufacturing Technology (AMT), Department of Science and Technology, New Delhi, India (sanction no. AMT/2017/082).

References:

[1] A. Sreenathbabu, K. P. Karunakaran, and C. Amarnath, "Statistical process design for hybrid adaptive layer manufacturing," Rapid Prototyping J., Vol.11, No.4, pp. 235-248, 2005.

[2] J. L. Z. Li, M. R. Alkahari, N. A. B. Rosli et al., "Review of Wire Arc Additive Manufacturing for 3D Metal Printing," Int. J. Automation Technol., Vol.13, No.3, pp. 346-353, 2019.

[3] J. S. Panchagnula and S. Simhambhatla, "Additive Manufacturing of Complex Shapes Through Weld-Deposition and Feature Based Slicing," Int. Mechanical Engineering Cong. and Exposition (ASME-IMECE 2015), V02AT02A004, 2015.

[4] L. Yuan, Z. Pan, D. Ding et al., "Fabrication of metallic parts with overhanging structures using the robotic wire arc additive manufacturing," J. Manuf. Process., Vol.63, pp. 24-34, 2021.

[5] P. Kazanas, P. Deherkar, P. Almeida et al., "Fabrication of geometrical features using wire and arc additive manufacture," Proc. Inst. Mech. Eng. (Part B: J. Eng. Manuf.), Vol. 226, No.6, pp. 1042-1051, 2012.

[6] J. P. M. Pragana, R. F. V. Sampaio, I. M. F. Bragança et al., "Hybrid metal additive manufacturing: A state-of-the-art review," Advances in Industrial and Manufacturing, Vol.2, 100032, 2021.

[7] G. Melis, P. Sirianni, A. Porceddu et al., "A Novel Platform for Smart 3D Manufacturing System," Int. J. Automation Technol., Vol.14, No.4, pp. 560-567, 2020.

[8] P. A. Colegrove, H. E. Coules, J. Fairman et al., "Microstructure and residual stress improvement in wire and arc additively manufactured parts through high-pressure rolling," J. Materials Processing Technology, Vol.213, No.10, pp. 1782-1791, 2013.

[9] H. Zhang, X. Wang, G. Wang et al., "Hybrid direct manufacturing method of metallic parts using deposition and micro continuous rolling," Rapid Prototyping J., Vol.19, No.6, pp. 387-394, 2013.

[10] F. Martina, P. A. Colegrove, S. W. Williams et al., "Microstructure of Interpass Rolled Wire + Arc Additive Manufacturing Ti-6Al-4V Components," Metallurgical and Materials Trans. A, Vol.46, Issue 12, pp. 6103-6118, 2015.

[11] Z. Hai-ou, R. Wang, L. Liang et al., "HDMR technology for the aircraft metal part," Rapid Prototyping J., Vol.22, No.6, pp. 857-863, 2016.

[12] J. Gu, J. Ding, S. W. Williams et al., "The strengthening effect of inter-layer cold working and post-deposition heat treatment on the additively manufactured Al–6.3Cu alloy," Materials Science and Engineering: A, Vol.651, pp. 18-26, 2016.

[13] X. Xu, S. Ganguly, J. Ding et al., "Enhancing mechanical properties of wire + arc additively manufactured INCONEL 718 superalloy through in-process thermomechanical processing," Materials & Design, Vol.160, pp. 1042-1051, 2018.

[14] Y. Xie, H. Zhang, and F. Zhou, "Improvement in Geometrical Accuracy and Mechanical Property for Arc-Based Additive Manufacturing Using Metamorphic Rolling Mechanism," J. Manuf. Sci. Eng., Vol.138, Issue 11, pp. 111002-111010, 2016.

[15] C. Ma, Y. Liu, C. Li et al., "Mechanical properties of carbon steel by compound arc and vibration shock forging-rolling," J. Manufacturing Processes, Vol.60, pp. 11-22, 2020.

[16] Y. Li and R. Rapthadu, "Bending-Additive-Machining Hybrid Manufacturing of Sheet Metal Structures," Proc. of the ASME 2017 12th Int. Manufacturing Science and Engineering Conf., Vol.1: Processes, V001T02A021, 2017.

[17] J. D. Kulkarni, S. B. Goka, P. K. Parchuri et al., "Microstructure evolution along build direction for thin-wall components fabricated with wire-direct energy deposition," Rapid Prototyping J., Vol.27, Issue 7, pp. 1289-1301, 2021.

[18] A. Ermakova, A. Mehmanparast, S. Ganguly et al., "Investigation of mechanical and fracture properties of wire and arc additively manufactured low carbon steel components," Theoretical and Applied Fracture Mechanics, Vol.109, 102685, 2020.

[19] S. Takushima, N. Shinohara, D. Morita et al., "In-Process Height Displacement Measurement Using Crossed Line Beams for Process Control of Laser Wire Deposition," Int J. Automation Technol., Vol.15, No.5, pp. 715-727, 2021.

[20] J. S. Panchagnula, A. Sharma, and S. Simhambhatla, "Thermal management in manufacture of thin-walled components produced by arc-based additive manufacturing," Proc. of the 10th Int. Conf. on Trends in Welding Research, 2016.

[21] L. D. Cozzolino, H. E. Coules, P. A. Colegrove et al., "Investigation of post-weld rolling methods to reduce residual stress and distortion," J. Materials Processing Technol., Vol.247, pp. 243-256, 2017.

Name:
Srinath Gudur

Affiliation:
Research Scholar, Department of Mechanical and Aerospace Engineering, Indian Institute of Technology Hyderabad (IITH)

Address:
Kandi, Sangareddy, Telangana 502285, India

Brief Biographical History:
2017- Research Scholar, IITH

Main Works:
• S. Gudur, S. Simhambhatla, and N. Venkata Reddy, "A Method and System to Fabricate a Component using Additive Manufacturing and Deformation Unit," Indian Patent, Application Number: 201941016062, 2020.
• S. Gudur, V. Nagallapati, S. Pawar, G. Muvvala, and S. Simhambhatla, "A study on the effect of substrate heating and cooling on bead geometry in wire arc additive manufacturing and its correlation with cooling rate," Materials Today: Proc., Vol.41, Part 2, pp. 431-436, 2020.

Name:
Suryakumar Simhambhatla

Affiliation:
Professor, Department of Mechanical and Aerospace Engineering, Indian Institute of Technology Hyderabad (IITH)

Address:
Kandi, Sangareddy, Telangana 502285, India

Brief Biographical History:
2010- Department of Mechanical and Aerospace Engineering, IITH

Main Works:
- Additive manufacturing of metallic objects, particularly large sized
- Hybrid techniques for AM (multi-process; multi-material form; multi-scale)
- Fabrication of functionally gradient objects through additive manufacturing
- Thermal balancing approaches for residual stresses and distortion control
- Medical applications of AM
- Industry 4.0 and circular manufacturing

Name:
N. Venkata Reddy

Affiliation:
Professor, Department of Mechanical and Aerospace Engineering, Indian Institute of Technology Hyderabad (IITH)

Address:
Kandi, Sangareddy, Telangana 502285, India

Brief Biographical History:
2012- Department of Mechanical and Aerospace Engineering, IITH

Main Works:
- Deformation processes
- Predictive models for digital fabrication
- Integrated product and process design systems
- Layered manufacturing